analytical chemistry

pubs.acs.org/ac Article

Native Ion Mobility–Mass Spectrometry-Enabled Fast Structural Interrogation of Labile Protein Surface Modifications at the Intact Protein Level

Gongyu Li,* Ashley Phetsanthad, Min Ma, Qinying Yu, Ashita Nair, Zhen Zheng, Fengfei Ma, Kellen DeLaney, Seungpyo Hong, and Lingjun Li*

Cite This: *Anal. Chem.* 2022, 94, 2142–2153 Read Online

ACCESS | Metrics & More | Article Recommendations | Supporting Information

ABSTRACT: Protein sialylation has been closely linked to many diseases including Alzheimer's disease (AD). It is also broadly implicated in therapeutics operating in a pattern-dependent (e.g., Neu5Ac vs Neu5Gc) manner. However, how the sialylation pattern affects the AD-associated, transferrin-assisted iron/Aβ cellular uptake process remains largely ill-defined. Herein, we report the use of native ion mobility–mass spectrometry (IM–MS)-based fast structural probing methodology, enabling well-controlled, synergistic, and in situ manipulation of mature glycoproteins and attached sialic acids. IM–MS-centered experiments enable the combinatorial interrogation of sialylation effects on Aβ cytotoxicity and the chemical, conformational, and topological stabilities of transferrin. Cell viability experiments suggest that Neu5Gc replacement enhances the transferrin-assisted, iron loading-associated Aβ cytotoxicity. Native gel electrophoresis and IM–MS reveal that sialylation stabilizes transferrin conformation but inhibits its dimerization. Collectively, IM–MS is adapted to capture key sialylation intermediates involved in fine-tuning AD-associated glycoprotein structural microheterogeneity. Our results provide the molecular basis for the importance of sustaining moderate TF sialylation levels, especially Neu5Ac, in promoting iron cellular transportation and rescuing iron-enhanced Aβ cytotoxicity.

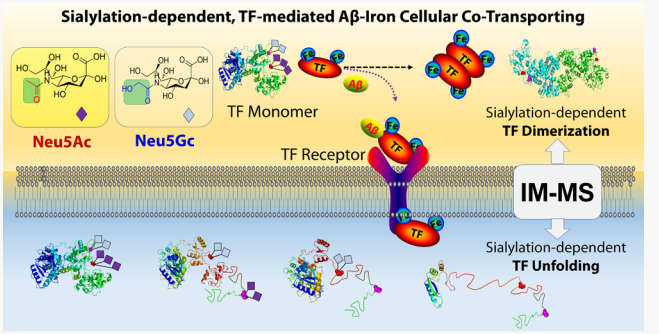

INTRODUCTION

The alteration of protein sialylation levels and patterns leads to severe biological impacts including increased cytotoxicity,[1] decreased cellular signaling activity,[2,3] and involvement in multiple prevalent diseases including carbohydrate deficient glycoprotein syndromes,[1] Parkinson's disease,[4] and Alzheimer's disease (AD).[5] One of such glycoproteins is the iron-carrier protein transferrin (TF), which has been found with altered sialylation levels in human cerebrospinal fluids and around senile plaques of the AD brain.[5−8] The alteration of TF sialylation levels and patterns may affect the iron homeostasis of the brain[5,7] and thus alter the surrounding brain environments that are tightly linked to AD dementia and progression.[9] Among the frequently sialylated glycoproteins, carrier proteins including serum TF[10] have attracted great interest owing to their central roles in transporting iron and significant regulatory roles that potentially act as supplementary diagnostic glycoproteins in multiple diseases.[11] Clearly, more definitive and experimental information would be beneficial for a better understanding of the relationship between altered sialylation of TF and iron homeostasis during AD development. However, currently, only limited molecular and structural information has been attainable for supporting the effects of sialylation on TF structure and dimerization.

Sialylation may have significant effects on the drug discovery and therapeutic treatments of AD. It has been demonstrated that the total glycoprotein sialylation and the identity of sialic acids [*N*-acetyl-neuraminic acid (Neu5Ac) and *N*-glycolyl-neuraminic acid (Neu5Gc)] regulate therapeutic protein efficacy, pharmacokinetics, and potential immunogenicity.[1] It has been well recognized that the human body mainly makes Neu5Ac rather than Neu5Gc, while in animals, for example, bovine can readily make both sialic acids. Notably, Neu5Gc modification, even with relatively low stoichiometry in human bodies, potentially exhibits significantly different impacts on protein structures and functions. However, it remains to be determined how sialylation affects the glycoprotein structure

Received: October 18, 2021
Accepted: January 5, 2022
Published: January 20, 2022

https://doi.org/10.1021/acs.analchem.1c04503
Anal. Chem. 2022, 94, 2142–2153

Scheme 1. Hypothetical Pathway for Iron and Aβ Cellular Transportation via the TF Cycle

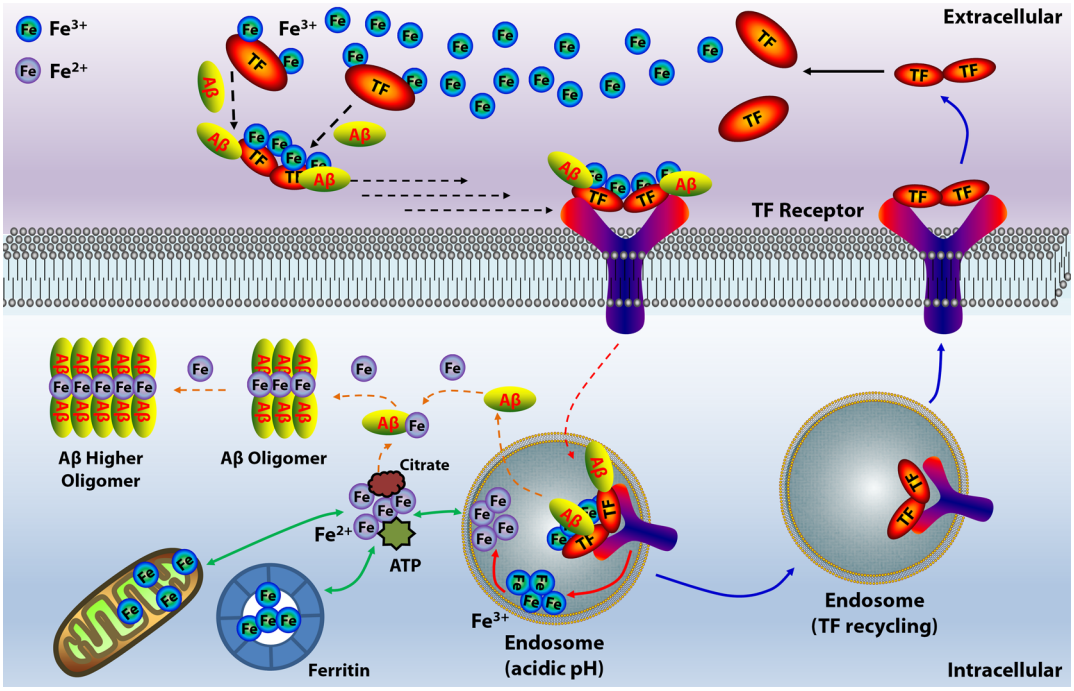

and thus function, and the extent to which Neu5Gc differs from Neu5Ac in terms of regulation of mature glycoprotein structures after being released from the endoplasmic reticulum is largely ill-defined.

The Robinson group has previously reported the effects of the global and site-specific *N*-glycan microheterogeneity on glycoprotein interactions by using native mass spectrometry (MS).[12] Though the sialylation effect was beyond their study, it has been clearly suggested that the negatively charged terminal sialic acids may change glycan orientations through extra steric hindrance or direct interaction with the protein backbone. In a more recent study, the ion mobility−MS (IM−MS) technique was used to correlate the stability of an immune scavenger protein with the number of its glycosylation site, where Neu5Ac was intensively involved.[13] Indeed, molecular dynamic simulation results have tentatively revealed the role of *N*-glycosylation at the C-lobe in regulating the 3D structure of TF as well as the impact of sialylation on *N*-glycan flexibility and conformation.[14,15]

As illustrated, Scheme 1 represents the widely acknowledged cartoon illustrations[10,16] of TF-assisted iron delivery into cells (note: the incorporation of amyloid beta (A*β*) has not been previously validated). Key steps involve the TF receptor-mediated endocytosis and internalization of iron-loaded TF, followed by iron redox, circulation, storage, and TF recycle. Under normal physiological conditions, cellular uptake of iron-loaded TF is driven by TF receptor-mediated endocytosis (Scheme 1, black arrow) in the luminal membrane of endothelial cells and internalization into endosomes (Scheme 1, red arrow). Ferric iron (Fe^{3+}) in endosome is partially reduced to ferrous iron (Fe^{2+}), while other Fe^{3+} and newly produced Fe^{2+} can be released from TF and recycled into cytoplasm. Upon iron release, TF is exported to the extracellular region and thus recycled (blue arrow) to bind Fe^{3+}. The unbound iron may enter mitochondria or be trapped and stored in protein ferritin in the brain cells (Scheme 1, green arrow) with high binding stoichiometry, thus mediating free iron concentration of the cytoplasm and nuclear compartments.[17]

Sequence alignment results (Figure S1) for TF among different species reveal the moderate sequence identity (∼58%) with 411 identical and 175 similar positions across human, bovine, and mouse TFs.[18] Frequently reported human TF *N*-glycosylation sites are Asn 432 and Asn 630, as indicated in Figure S1, while bovine and mouse TF glycosylation sites are identical in alignments.[19,20] A markedly known difference among human, bovine, and mouse TFs is the varied sialylation number and pattern, for example, human TF with up to four Neu5Ac but bovine and mouse TFs with varied numbers of Neu5Ac and Neu5Gc.[6,10,21] Differentially sialylated TF isoforms, for example, desialylated versus one to four Neu5Ac-attached, in combination with the presence of both biantennary and triantennary *N*-glycan patterns, make TF highly heterogenous and thus challenging to characterize. It would also be interesting to interrogate how this type of heterogeneity affects the protein TF structure, interaction, and downstream functions.

Herein, cell viability measurements were first performed to examine the TF sialylation-mediated A*β* cytotoxicity. Starting with the functional interrogation of sialylation-regulated cellular transportation of iron and A*β* via the TF cycle (Scheme 1), native IM−MS was then employed to effectively and confidently dissect the sialylation effects on the overall 3D arrangements of TF, including chemical, conformational, and topological stabilities. While bottom-up proteomics was employed to accurately determine the specific sialylation patterns in various TF samples, native gel electrophoresis experiments further extended our gas-phase findings to solution phase. Taken together, this study provides a molecular basis for the importance of TF sialylation, especially Neu5Ac, in promoting iron cellular transportation and rescuing iron-enhanced A*β* cytotoxicity. These new findings also potentially provide supplementary molecular clues for TF-mediated cell

https://doi.org/10.1021/acs.analchem.1c04503
Anal. Chem. 2022, 94, 2142−2153

ferroptosis in disease progression, adding to the recently reported chemical basis for ferroptosis.[22]

EXPERIMENTAL DETAILS

Chemicals. Protein samples (including human/bovine/mouse transferrin) and necessary buffer salts were obtained from Sigma-Aldrich (St. Louis, MO). Detailed information for protein samples is as follows: human transferrin, item #T3309, ≥ 98%; holo-transferrin human, item #T4132, ≥ 98%; apo-transferrin bovine, item #T1428, ≥ 98%; and apo-transferrin from mouse, item #T0523, ≥ 98%. Materials for gel electrophoresis including 30% acrylamide/bis (19:1) solution, Bio-Rad Precision Plus Protein Dual Color Standards, ammonium persulfate, TEMED, and 4× Laemmli Sample Buffer were bought from Bio-Rad Laboratories, Inc. 6-Aminohexanoic acid, Bis-Tris, Coomassie brilliant blue G 250, Tricine, Tris Base, Triton X-100, β-mercaptoethanol, and sodium dodecyl sulfate (SDS) were purchased from Sigma-Aldrich. No further purification was performed for the reagents. All solvents used in this study were of HPLC grade supplied by Sigma-Aldrich (St. Louis, MO). Purified water (conductivity of 18.2 MΩ cm) was obtained from a Milli-Q Reference System (Millipore Corp., Bedford, MA, USA).

Blue Native Polyacrylamide Gel Electrophoresis. The gel electrophoresis was carried out with procedures as stated elsewhere.[23] The protein separations in their native state were done with a 4−16% gradient acrylamide gel prepared in house using Bis-tris buffer at pH 7.0. Purified protein samples of 10 μg were mixed with a concentrated solution of loading buffer at a ratio of 9:1 to achieve final concentration of 50 mM 6-aminohexanoic acid, 0.5% w/v of Coomassie brilliant blue G250, 10% v/v of glycerol, and 0.1% v/v Triton X-100. The buffers used for electrophoresis were cathode buffer I (50 mM tricine, 0.02% w/v of Coomassie brilliant blue G250, and 50 mM Bis-Tris at pH 7.0), cathode buffer II (50 mM tricine, 0.002% w/v of Coomassie brilliant blue G250, and 50 mM Bis-Tris at pH 7.0), and anode buffer (50 mM Bis-Tris at pH 7.0). The cathode buffer I was changed to cathode buffer II after half the run time. Electrophoresis of the samples was done at 150 V at 4 °C. The gel was, subsequently, fixed and destained with a solution of 50% water, 40% methanol, and 10% acetic acid till a clear background was achieved. Bovine serum albumin (BSA, monomer at 66 kDa, dimer at 132 kDa), catalase (250 kDa), and fibrinogen (340 kDa) were used as molecular weight markers.

SDS Polyacrylamide Gel Electrophoresis. The protein separations in their denatured state were done with a 4−16% gradient acrylamide gel under reducing and denaturing condition. 10 μg of purified protein samples was mixed with 4× Laemmli sample buffer containing β-mercaptoethanol at a 3:1 ratio and heated for 5 min at 95 °C. Electrophoresis was done at 100 V using 1× running buffer (0.025 M Tris, 0.192 M glycine, 0.1% SDS at pH 8.3). The gel was, subsequently, stained with 0.025% w/v Coomassie brilliant blue G250 in 10% acetic acid followed by de-staining with a solution of 50% water, 40% methanol, and 10% acetic acid till a clear background was achieved. BioRad Precision Plus Protein Dual Color Standards was used as a molecular weight marker.

Cell Viability Measurements (MTT Assay). MTT experiments were carried out following similar protocols with previous report.[24] The human neuroblastoma Neuro-2a (N2a) cell line was purchased from the American Type Culture Collection (ATCC, Manassas, VA, USA). The cell line was maintained in media containing 1:1 Minimum Essential Media (MEM, GIBCO, Grand Island, NY, USA) and Ham's F12K Kaighn's Modification Media (F12K, GIBCO), 10% (v/v) fetal bovine serum (Sigma-Aldrich), and 1% (v/v) penicillin (GIBCO). The cells were grown and maintained at 37 °C in a humidified atmosphere with 5% CO_2. Cell viability upon treatment of Aβ with or without Fe^{3+} and/or TF was determined by the MTT assay. N2a cells were seeded in a 96-well plate (15,000 cells in 100 μL per well) and treated with pre-incubated (20 h) Aβ (10 μM), $FeCl_3$ (10 μM), and/or TF (~5 μM). After 24 h incubation at 37 °C, 100 μL MTT (0.5 mg/mL in phosphate buffered saline and DMEM media) was added to each well and the plates were incubated for 2 h at 37 °C. The MTT solution was removed by a multichannel pipette, and then, 100 μL of DMSO was added to the culture well. It was gently mixed in a gyratory shaker or pipetted up and down. The absorbances at 570 and 690 nm were measured on a microplate reader. The optical density (OD) of each well was measured by subtracting absorbance at 690 nm from absorbance at 570 nm. The relative viability (RV) was measured by the following formula

$$\mathrm{RV} = \frac{\mathrm{OD\ of\ sample} - \mathrm{OD\ of\ blank\ control}}{\mathrm{OD\ of\ negative\ control} - \mathrm{OD\ of\ blank\ control}} \times 100\%$$

Glycoprotein Enzymatic Digestion. The characterization of sialylation patterns in three transferrin proteins (human, bovine, and mouse transferrin) was carried out with the following procedures: human, bovine, and mouse transferrin were reconstituted in 8 M urea buffer in 50 mM Tris base. To reduce disulfide bonds, 100 mM DTT was added to the protein to a final concentration of 5 mM and the mixture was incubated at room temperature for 1 h. Then, 200 mM IAA was added to a final concentration of 15 mM and incubated for 30 min at room temperature in the dark. The reaction was quenched by adding 100 mM DTT and incubating for 5 min at room temperature. 50 mM Tris base was added to reduce urea concentration to 1 M or less to avoid trypsin inhibition. Finally, trypsin (protein/enzyme = 50:1) was added to the protein and the mixture was incubated at 37 °C overnight. Digestion was terminated by adding trifluoroacetic acid to a final concentration of 0.25%, and particulate material was removed by centrifuging at 14,000g for 10 min. A sample mixture was desalted using a SepPak C18 SPE cartridge (Waters, Milford, MA). The cartridge was conditioned with 1 mL of ACN and 3 mL of 0.1% trifluoroacetic acid in H_2O. The sample mixture was reconstituted in 500 μL of 0.1% trifluoroacetic acid in H_2O and added to the conditioned cartridge. The cartridge was then washed with 1.5 mL of 0.1% trifluoroacetic acid in H_2O, and peptides were step-wisely eluted with 900 μL of 50% ACN, 0.2% formic acid in H_2O, followed by 700 μL of 70% ACN, 0.2% formic acid in H_2O. The eluting fraction was dried in vacuo, reconstituted in 3% ACN, 0.1% formic acid in H2O, and analyzed by LC−MS/MS.

Liquid Chromatography with Tandem Mass Spectrometry. A Dionex Ultimate 3000 nanoLC system was coupled to an Orbitrap Fusion Lumos Tribrid quadrupole-ion trap-Orbitrap mass spectrometer with a NanoSpray Flex ion source (Thermo Scientific, Bremen, Germany) for all LC−MS/MS analyses. A binary solvent system composed of H_2O containing 0.1% formic acid (A) and ACN containing 0.1% formic acid (B) was used for all analyses. Peptides were loaded

https://doi.org/10.1021/acs.analchem.1c04503
Anal. Chem. 2022, 94, 2142−2153

and separated on a self-fabricated 75 μm × 15 cm column packed with 1.7 μm, 130 Å, BEH C18 material obtained from a Waters UPLC column (part no. 186004661). The LC gradient was set as follows: 3−30% A (18−108 min), 30−75% A (108−118 min), and 75−95% A (118−128 min). The mass spectrometer was operated in data-dependent mode using a topN approach (top 20 precursors). The HCD-triggered EThcD acquisition method was employed. MS1 scan was acquired from 400 to 1800 (120,000 resolving power, 4×10^5 AGC, 50 ms injection time) followed by HCD MS/MS acquisition of the precursors in the Orbitrap (30,000 resolution, 5×10^4 AGC, 54 ms injection time). EThcD was performed only when at least two of the oxonium ions (m/z 138.055, 168.065, 204.087, and 366.140) were detected in the HCD MS/MS spectra. EThcD spectra was acquired with the following parameters: 60,000 resolving power, 2×10^5 AGC, 250 ms injection time with an optimized user-defined charge-dependent reaction time (2+, 200 ms; 3+, 200 ms; 4+, 200 ms; 5+, 200 ms) supplemented by 33% HCD activation.

Bottom-Up Proteomics Data Analysis. All raw data files from human, bovine, and mouse transferrin were searched against UniProt homo sapiens reviewed database (08.10.2016; 20,152 sequences), UniProt Bos Taurus reviewed database (06.09.2017; 6,367 sequences), and UniProt *Mus musculus* reviewed database (08.13.2016; 24,903 sequences), respectively. PTM-centric search engine Byonic (version 3.3.11, Protein Metrics, San Carlos, CA) incorporated in Proteome Discoverer (PD 2.1) was used. Trypsin was selected as the enzyme, and two maximum missed cleavages were allowed. Searches were performed with a precursor mass tolerance of 10 ppm and a fragment mass tolerance of 0.01 Da. Static modifications consisted of carbamidomethylation of cysteine residues (+57.02146 Da). Dynamic modifications consisted of oxidation of methionine residues (+15.99492 Da), deamidation of asparagine and glutamine (+0.98402 Da), and *N*-glycosylation on asparagine. Oxidation and deamidation were set as "rare" modification, and *N*-glycosylation was set as "common" modification through Byonic node. Two rare modifications and one common modification were allowed. Human *N*-glycan database embedded in Byonic, which contains 182 glycan entities and mammalian *N*-glycan database with 309 glycan entities were used. Only *N*-glycopeptides with PSMs with an FDR ≤ 1% and Byonic score over 50 were reported, and such criteria were set based on the expertise experience of manual spectra check and previous evaluation of the software. Each glycopeptide identified should have the consensus motif NX/T/S, X≠P.

Sialylation Pattern Determination. *N*-glycans were released from human, bovine, and mouse transferrin with a slightly modified filter-aided *N*-glycan separation strategy (PMID: 26086806). Glycoproteins were dissolved in water and mixed with TCEP. Heat denaturation was performed by switching sample tubes between 100 °C and room temperature water baths for four cycles of 15 s each. The mixture was then loaded onto a 30 kDa molecular weight cutoff (MWCO) filter and buffer-exchanged with triethylammonium bicarbonate buffer (TEAB) by centrifugation to remove contaminants with low molecular weight. PNGase F was added to each filter and incubated at 37 °C overnight. *N*-Glycans were separated with deglycosylated proteins and eluted by centrifugation. The filter was then washed with TEAB buffer to ensure complete elution of *N*-glycans. Fractions were combined and dried in vacuo.

N-Glycans were subjected to linkage-specific derivatization following a previous protocol (PMID: 24831253). Briefly, glycans were added to ethanol containing EDC and HOBt. Samples were incubated for 4 h at 37 °C. Sample cleanup was performed through cotton hydrophilic interaction liquid chromatography solid phase extraction, as described previously (PMID: 21366235). Derivatized *N*-glycans were analyzed using a rapifleX mass spectrometer (Bruker Daltonik GmbH).

α2,6-linked sialic acids undergo esterification, whereas α2,3-linked sialic acids can instead form an intramolecular lactone, leading to water loss. The resulting mass difference allows the direct distinction of sialic acid linkages by mass spectrometry.

De-Sialylation of Glycoprotein Transferrin. To study the effects of sialylation on the glycoprotein structure and dimerization, fully sialylated human/bovine/mouse transferrins were de-sialylated by using sialidase of neuraminidase under native conditions. Neuraminidase (Sialidase, from *C. Perfringens* 11585886001 Roche) was supplied by Sigma-Aldrich (St. Louis, MO). First, the enzyme is dissolved/reconstituted to 5 mL of water (Sialidase concentration: 1 U/mL). Then, in a 600 μL centrifuge tube, 100 μL of glycoprotein (human/bovine/mouse transferrin, 1 mg/mL in 100 mM NH_4OAc, pH 7) and then 100 μL of NaOAc (0.1 M, pH 5) were added. After that, 25 μL of BSA (0.5 mg/mL) was added for enzyme stabilization. Then, 25 μL of sialidase (1 U/mL) was added, while for the control group, 25 μL of NaOAc (0.1 M, pH 5) was added instead. After vortex mixing and parafilm sealing, the mixtures of 250 μL were incubated in a water bath at 37 °C for 5 h. The de-sialylation reaction was finally stopped with the addition of 25 μL of $NaHCO_3$ (0.5 M). After de-sialylation, proteins were buffer-exchanged into 100 mM NH_4OAc with Amicon Ultra-0.5 Centrifugal Filter Devices [30 kDa MWCO: UFC503024, Sigma-Aldrich (St. Louis, MO)] following the procedures given below.

All-Ion Native IM−MS. Each sample of approximately 5 μL (~8 μM glycoproteins in 100 mM ammonium acetate) was loaded into a home-made nanospray ion source, and a silver wire of 100 μm thickness was inserted into the borosilicate glass needle for high voltage application. Nanospray voltages ranged between 1.0 and 2.0 kV. In typical nanospray experiments, the size of the spray emitter was maintained at ~5 μm. The nanospray needles were pulled from borosilicate glass capillaries using a P-2000 laser-based micropipette puller (Sutter Instruments, Novato, CA, USA). The MS instrument was run in positive ion mode, and the sampling cone was used at 30 V. All IM−MS data were collected using Waters Synapt G2 instruments. The MS cone temperature was 70 °C. The Synapt G2 instrument was tuned to allow for preservation and transmission of native proteins and protein interactions. This typically involves elevated pressures in the source region (~6 mbar) and decreasing all focusing voltages (e.g., cone, extractor, and bias voltages). The traveling-wave IM separator was operated at a pressure of ~3.5 mbar, and DC voltage waves (30 V wave height traveling at 400 m/s) to induce IM separation. All ion fragmentation (AIF) was achieved by increasing the trap CE from 10 to 180 V with a step voltage of 5 or 10 V, while no precursor ion selections by quadrupole were made throughout the experiments in this study.

IM−MS Data Analysis. The TOF-MS was typically operated over the m/z range of 400−8000. CCS calibration curves were generated using a previously described protocol and using literature CCS values with nitrogen (N_2) derived for use with the Synapt instrument platform.[25,26] The theoretical

https://doi.org/10.1021/acs.analchem.1c04503
Anal. Chem. 2022, 94, 2142−2153

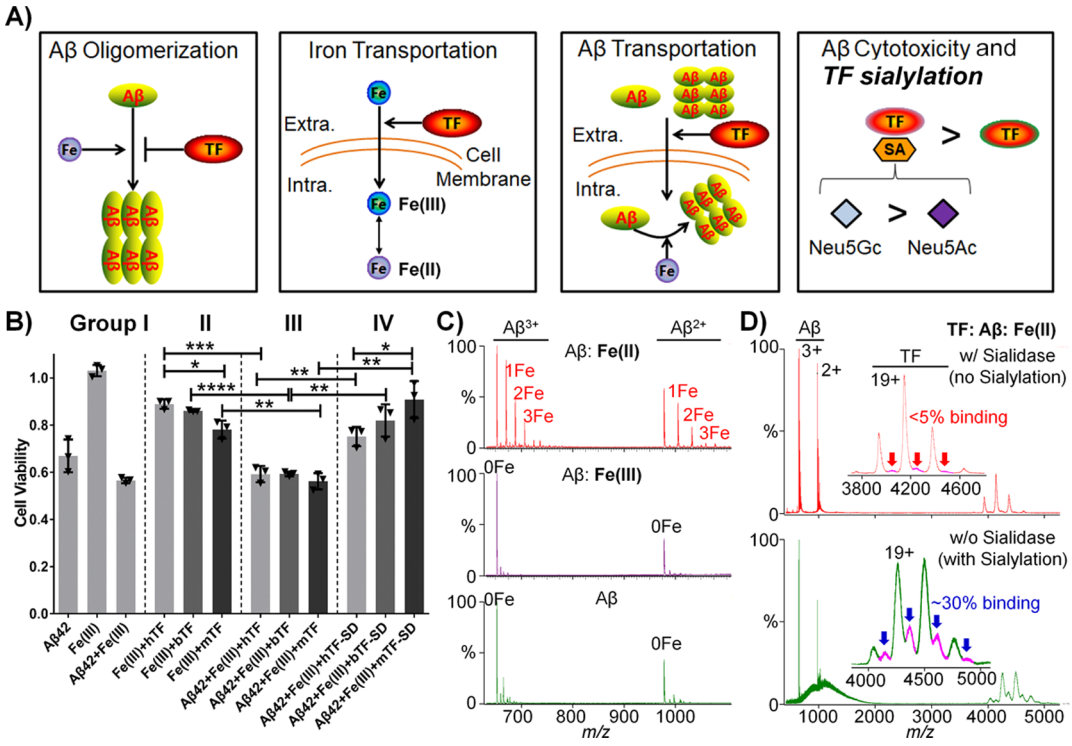

Figure 1. TF sialylation-dependent Aβ cytotoxicity. (A) Cartoon illustrations of Aβ oligomerization, iron transportation, and Aβ transportation under the influence of TF. In addition, the observed Aβ cytotoxicity was also shown as a function of the TF sialylation pattern. (B) MTT-based cell viability tests for iron-enhanced Aβ cytotoxicity and recovery by TF with varying sialylation termini. Definition of hTF/bTF/mTF, human/bovine/mouse TF, SD, and sialidase (an enzyme to remove sialic acid). Error bars, S.D. (n = 3). Statistical measurements are based on unpaired two-tailed Student's t-test. *$P \leq 0.05$; **$P \leq 0.01$; ***$P \leq 0.001$; ****$P \leq 0.0001$. (C) Native MS data for selective Aβ−iron binding events. Aβ, 10 μM; Fe(II)/Fe(III), 20 μM; buffer, 10 mM ammonium acetate. (D) Native MS data for sialylation-dependent human TF-Aβ binding events, supporting sialylation-mediated co-importing of Aβ and iron. To simplify the binding system, the Aβ (1−16) fragment is selected as a model Aβ peptide as the iron binding domain is located at the N-terminus.

CCS values from helium were obtained from IMPACT calculation with PDB ID of 2HAV.[27] To generate the CIU fingerprints, only the data at m/z values corresponding to the selected charge state of the precursor ions were selected for analysis. As previously reported,[28] once the amount of parent ion was less than five percent of the total signal, the CIU fingerprinting experiments were terminated. The data were normalized at each voltage through dividing the intensities of ions at each drift time by the maximum ion intensity observed at that voltage. CIUSuite is a series of Python modules for the generation and manipulation of CIU fingerprints, which is developed by the Ruotolo Research Group[29] at the University of Michigan. CIU fingerprints, subsequent CIU50 and RMSD calculations, and feature analysis were carried out using CIUSuite. UniDec is a data analysis package that employs a Bayesian framework to separate the mass and charge dimensions, resulting in the rapid and robust visualization of mass spectra and IM-MS developed by the Robinson Research Group[30] at the University of Oxford. AIF mass spectra were generated by using UniDec without further modifications except necessary optimization of UniDec parameters, like charge range, mass range, sample mass frequency, peak FWHM, and peak selection, and plotting parameters like peak detection range and peak detection threshold.

Statistical Analysis. Student's t-test was used to evaluate statistical significance of the observed cytotoxicity differences among different Aβ groups.

RESULTS AND DISCUSSION

Sialylation Effects in the Transferrin Cycle. Figure 1A summarizes the potential roles of TF in Aβ oligomerization, iron transportation, Aβ transportation, and observed Aβ cytotoxicity under the regulation of the sialylation pattern. On top of widely adopted iron cellular transportation via the TF cycle,[10,16] we propose here that Aβ can also be transported into cells via TF-assisted endocytosis (Scheme 1). A detailed pathway for iron cellular transportation via TF and proposed Aβ escape routes presumably through proton sponge effects[31] from endosome upon cellular uptake via TF can be found in Scheme 1. It has been reported that TF can inhibit Aβ oligomerization,[32] while iron seems to promote Aβ oligomerization.[33,34] Our cytotoxicity experiments (Figure 1B, see below for details) suggest that TF with sialylation enhances Aβ cytotoxicity, while Neu5Gc seems to have a more profound effect than Neu5Ac. IM−MS results (Figures 1C,D and S2 and S3) indicate that TF with sialylations holds high affinity to both iron and Aβ, which may provide a molecular basis for its high-efficiency transmembrane translocation and potential endosome escaping routes as indicated by the pH-dependent binding events among TF, iron, and Aβ. Based on the abovementioned previous reports, together with our collective molecular observations and cell experiments (details as shown below), we hypothesize that sialylation promotes enhanced cellular transportation of Aβ and iron via the TF cycle.

Notably, the TF-assisted co-importing is substantially supplementary to the direct receptor-mediated endocytosis of

https://doi.org/10.1021/acs.analchem.1c04503
Anal. Chem. 2022, 94, 2142−2153

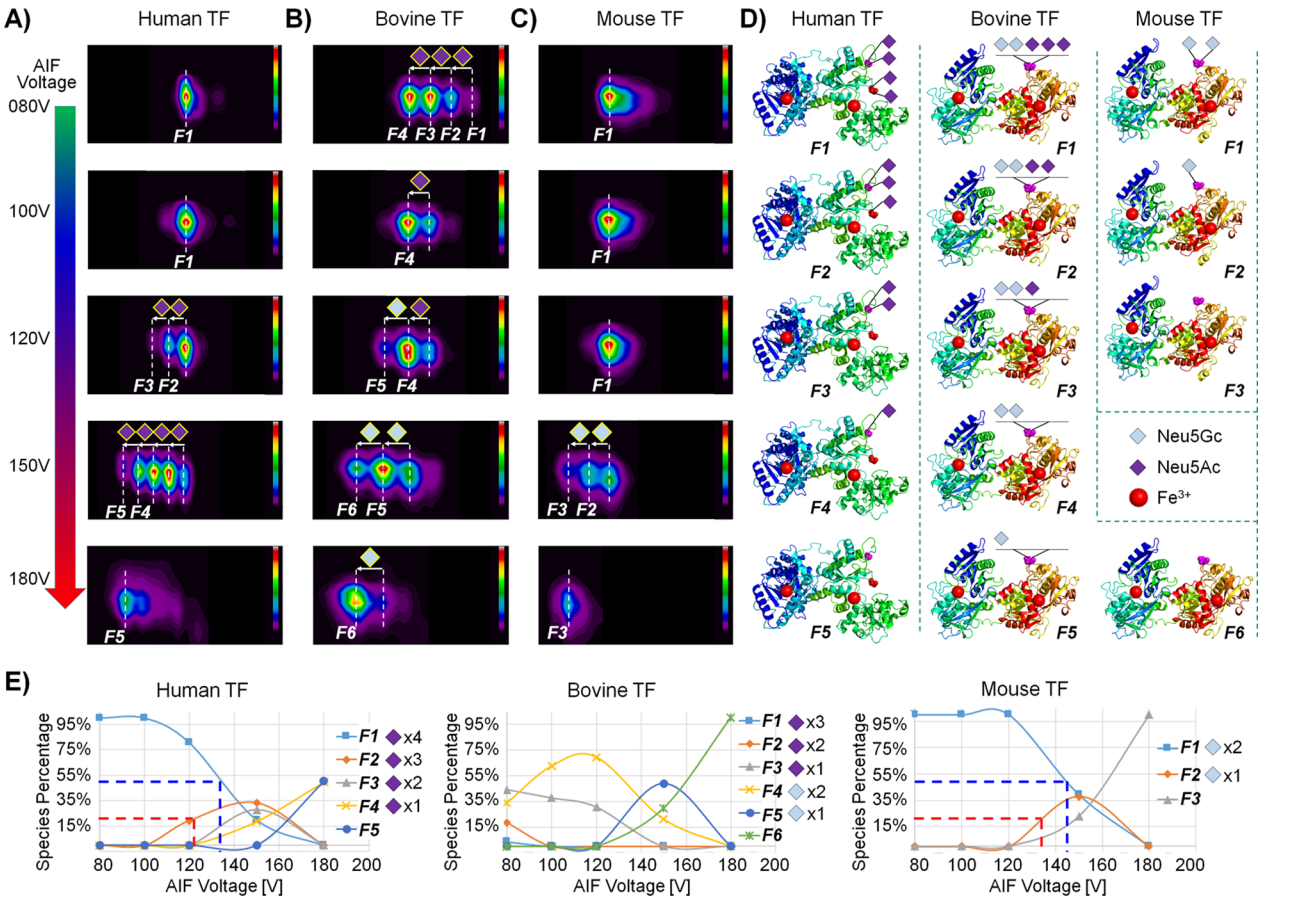

Figure 2. Stepwise releasing of sialic acids from holo-transferrin. Snapshots of representative AIF results from human, bovine, and mouse TFs are shown in (A−C), respectively. Note, charge distribution (*y*-axis) and mass distribution (*x*-axis). (D) Key sialylation patterns (human TF, F1−F5; bovine TF, F1−F6; mouse TF, F1−F3) are illustrated for these TF glycoproteins based on different models: human (PDB ID: 2HAV); bovine (AlphaFold: AF-Q29443-F1-model_v2); and mouse (AlphaFold: AF-Q921I1−F1-model_v2). (E) Species percentages for these TF glycoproteins as a function of AIF energy as derived from AIF images (A−C). Intensity scale bars in (A−C) are from 0 to 100%. All glycoproteins are in apo-forms. The measured molecular weights of different sialylation forms are 79.69/79.39/79.09/78.79/78.49 kDa, 79.03/78.73/78.43/78.13/77.84/77.55 kDa, and 77.30/77.01/76.72 kDa for human, bovine, and mouse TFs, respectively. Neu5Ac and Neu5Gc releasing induces mass shifts of 291 and 307 Da, respectively.

Aβ and iron, especially when considering its cytotoxicity associated with oligomers rather than Aβ monomer. It will thus be more interesting to directly evaluate the sialylation effects on the biological functions of glycoprotein TF in the presence of Aβ.

TF Sialylation-Conferred Iron/Aβ Cytotoxicity. As TF is primarily involved in iron homeostasis, we thus focus on the sialylation effects on the iron-regulated Aβ cytotoxicity, which is believed to be linked to the pathology of neurodegenerative disease.[6,34,35] Cytotoxicity is examined by using an MTT assay similar to a previous report[24] on a N2A cell line. From MTT assay experiments in Figure 1B, sole addition with Aβ42 leads to significant cell death as indicated by the decreased cell viability values (group I). The cell viability for the Aβ42 treatment group is slightly decreased (group I, Figure 1B) upon adding ferric iron, suggesting an increase in cytotoxicity through interaction with iron. The observation that Aβ42 cytotoxicity is enhanced by incubation with Fe^{3+} has also been observed in a previous report.[33] However, both previous NMR observations[36,37] and our native IM−MS data (Figure 1C) have confirmed the preferential binding of Aβ to ferrous iron (Fe^{2+}) rather than ferric iron (Fe^{3+}). We suspect that Aβ and Fe^{3+} are co-imported into cells, where Fe^{3+} is reduced to Fe^{2+} that can directly bind with Aβ. Consequently, the direct Aβ−iron interaction may promote the formation of toxic oligomers, which is also in line with previous observations.[33]

In order to evaluate the effects of sialylation pattern (type and number of terminal sialylations) on TF activity during Aβ infection, three types of TF (human-derived, bovine-derived and mouse-derived) are used in cell viability experiments. To simplify the system and obtain more stable native MS signals, in Figure 1C,D, we chose Aβ (1−16) instead of Aβ42 that is used in cell experiments (Figure 1B), as Aβ (1−16) is much easier to dissolve in water and has thus better MS compatibility than Aβ42. Moreover, the iron binding domain is located at the *N*-terminus of Aβ42,[36,37] which makes Aβ (1−16) a good model to investigate the effect of iron binding on the structural effect. Notably, cell incubation with Fe^{3+} alone is nontoxic (group I, Figure 1B). However, overloading of Fe^{3+} by TF is more toxic (group II, Figure 1B). As indicated by the differential cell viabilities, Neu5Gc-rich mouse TF with a cell viability of ∼78% seems to overload more Fe^{3+} compared to Neu5Ac-rich human TF with a cell viability of ∼88%. Meanwhile, the cytotoxicity of TF-mediated iron overloading is significantly enhanced with the co-imported Aβ42 (group III, Figure 1B). While all the samples in group III show less

https://doi.org/10.1021/acs.analchem.1c04503
Anal. Chem. 2022, 94, 2142−2153

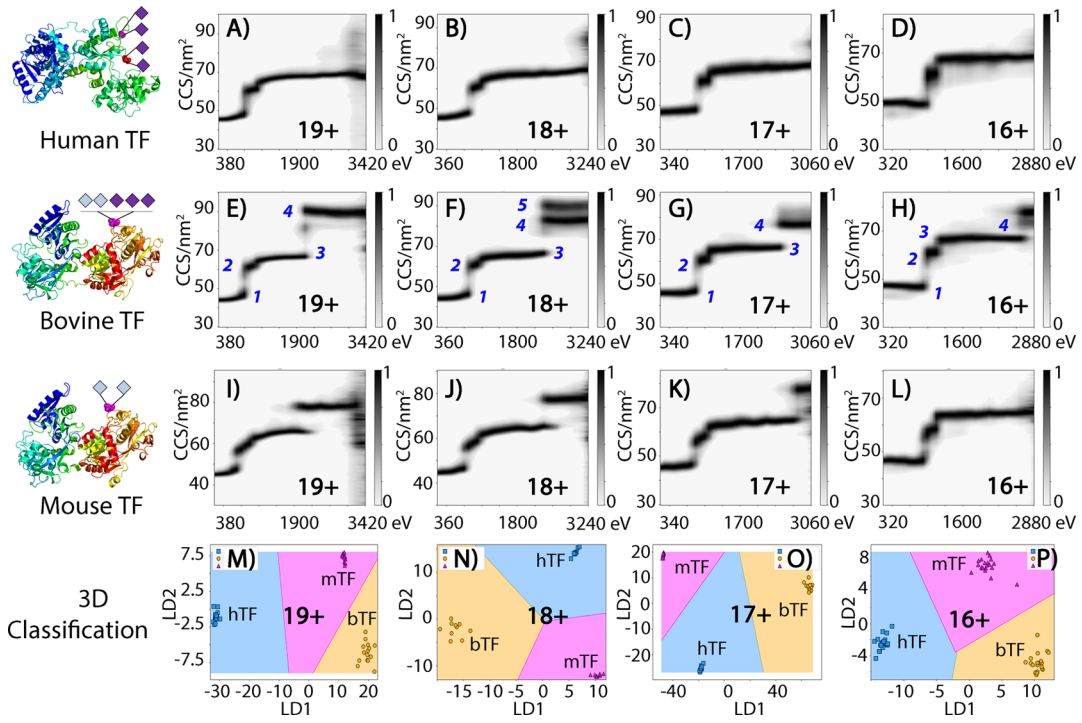

Figure 3. Sialylation-conferred apo-transferrin stepwise unfolding. Unfolding fingerprints for differentially sialylated glycoproteins, human (A−D), bovine (E−H), and mouse (I−L) TFs are shown as a function of lab-frame collision energy (CE). Human, bovine, and mouse TF fingerprint 3D classification results for 19+ (M), 18+ (N), 17+ (O), and 16+ (P). Numbers (1−5) in (E−H) represent different conformations. All fingerprints are extracted from mass-resolved fully sialylated glycoforms. Calculation of lab-frame CE is detailed in Supporting Information and Table S1.

than 60% cell viability, hTF, bTF, and mTF with different sialylations exhibit different levels of cell viability change against the co-imported Aβ42. It should be noted that the cytotoxicity of the Aβ42/iron/TF mixture is derived from a composite effect of iron overloading, Aβ42 oligomerization, and the cross-talk effects between Aβ42 and intracellularly reduced Fe^{2+}.

To further interrogate the differential roles of Neu5Ac and Neu5Gc, we employ an enzymatic removal strategy to release sialic acids by using sialidase.[21] Mass difference of apo-human TF (Figures 1D and S4) induced by sialidase treatment is 1234 ± 22 Da (n = 3), suggesting a complete removal of four Neu5Ac (mass of 309 Da) in human TF by using sialidase. Generally, removal of sialylation differentially rescues the N2A cells from cytotoxicity of the Aβ42/iron/TF mixture (group IV, Figure 1B). Under the influence of human TF without sialylation (after sialidase treatment), the cytotoxicity of Aβ42 is effectively alleviated, which is probably due to the participation of human TF in mediating Aβ cellular transportation, where only a small amount of Aβ was co-imported into cells along with Fe^{3+} without sialylation (w/sialidase, top spectrum in Figure 1D). Interestingly, sialylation modification of TF significantly increases Aβ binding to TF (w/o sialidase, bottom spectrum in Figure 1D) and thus may be related to the enhanced co-importing of Aβ, which further explains why removal of sialylation rescues N2A cells. The cell viability elevation for de-sialylation rescuing of the mouse TF group is significantly higher than that of human TF. This observation along with the much higher viability of sialidase-treated mouse TF compared to sialidase-treated human TF (group IV, Figure 1B) revealed that Neu5Gc-rich TF bears much higher inhibitory effects during cell growth than that of Neu5Ac-rich TF. Collectively, although de-sialylation of both Neu5Ac and Neu5Gc alleviates the burden from Aβ cytotoxicity, Neu5Ac modification tends to be more beneficial for TF in maintaining cell viability and shows less profound effects than Neu5Gc on accumulating Aβ cytotoxicity.

In the following sections, we aim to understand the molecular mechanism underlying the differential roles of the sialylation pattern (Neu5Ac/Neu5Gc) in regulating the TF structure and topology, through some modifications with the state-of-art IM−MS techniques and other biophysical tools.

Chemical Stability Analysis of Differentially Sialylated Transferrin. The rationale of the method of choice for nontargeted AIF-equipped native IM−MS strategy is described in Supporting Information. The key step in unveiling sialylation effects on glycoproteins is to interrogate its chemical stability from differentially sialylated TF proteins. The gas-phase dissociation is thus used to track the thermal stability of sialylation modification; this technique has been demonstrated suitable for mapping solution structural feature of proteins.[26,38] Representative nontargeted AIF−MS snapshots of holo-human TF at various AIF voltages are shown in Figures S5A and S6. Distinct gradual release of sialic acids is observed throughout different charge states (Figure S5B) of TF ions along with the elevation of activation energy, as indicated by a corresponding stepwise mass shift of 291 Da (Neu5Ac sialylation mass).

A series of bottom-up experiments were performed to confidently validate the sialylation patterns (Figures 2A−C, S7−S13 and Table S2) and linkages (Figure S14) for all three TF protein systems. We employed electron-transfer/higher-energy collision dissociation (EThcD) to facilitate bottom-up sequencing of both the primary structure (Figures S7−S9) and the sialylation patterns (Figures S10−S13 and Table S2). In all cases, protein sequence coverage is more than 88%, with a list of glycol isoforms being identified for each of these three TFs

https://doi.org/10.1021/acs.analchem.1c04503
Anal. Chem. 2022, 94, 2142−2153

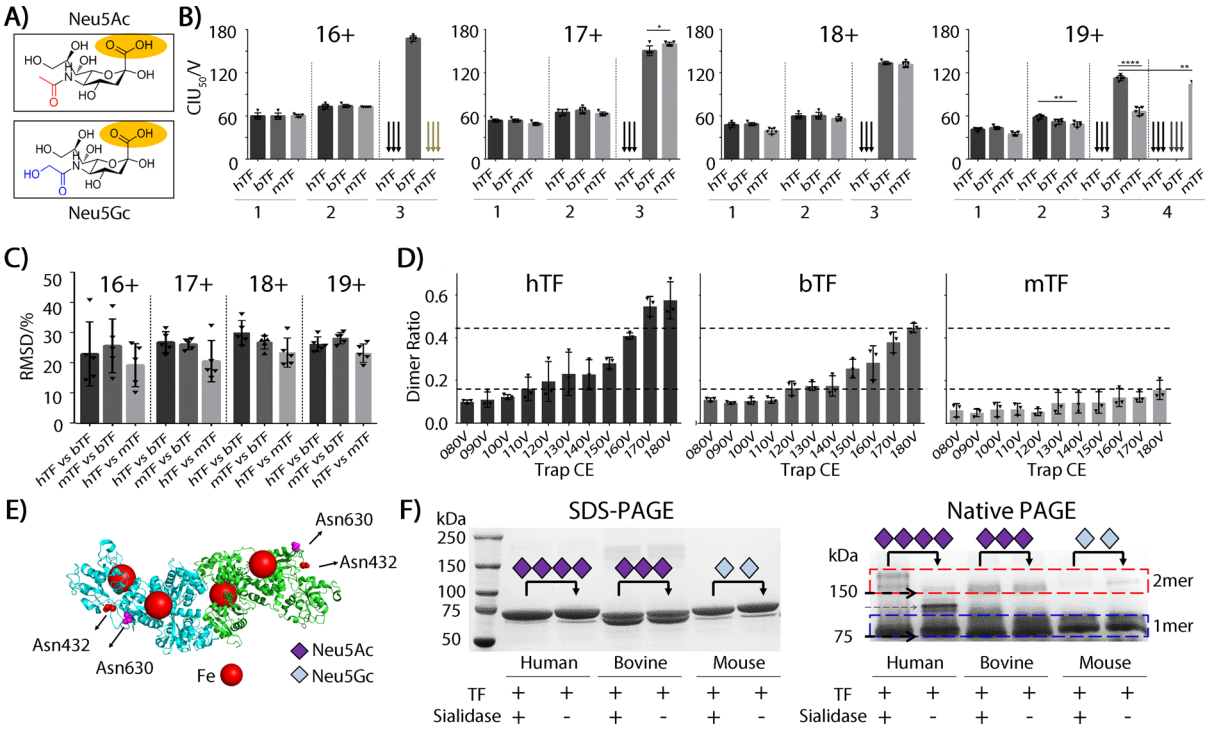

Figure 4. Molecular evidence of sialylation effects. (A) Chemical structures of two sialic acids, Neu5Ac and Neu5Gc, with highlights of an acidic group and difference in a hydroxyl group. (B) Conformational stability analysis of apo-TF as a function of sialylation pattern revealed by CIU50 values of multiple transitions (19+, 4 transitions; 16+/17+/18+, 3 transitions). Error bars, S.D. (n = 5). Statistical measurements are based on unpaired two-tailed Student's t-test. *$P \leq 0.05$; **$P \leq 0.01$; ****$P \leq 0.0001$. Arrows, no CIU50 for these transitions. (C) Overall structural comparison for apo-TF with different sialylation types revealed by RMSD values derived from unfolding difference plots. All error bars denote standard deviation from five independent experiments. (D) Dimer ratios change as a function of holo-TF sialylation releasing energy. All error bars denote standard deviation from three independent experiments. (E) Cartoon illustrations of the crystal structure for holo-human TF dimer (derived from PDB entry: 2HAV). (F) In-solution identification of the sialylation effects on holo-TF dimerization revealed by SDS polyacrylamide gel electrophoresis (PAGE) and native PAGE. Note, a band of 132 kDa corresponding to BSA dimer is observed in the group of human TF without sialidase in the native PAGE.

(Table S2). Glycoproteomics data unambiguously identify two *N*-glycosylation sites, Asn 432 and Asn 630 of human TF with purely Neu5Ac attached at the end, confirming that no Neu5Gc but only Neu5Ac is attached to human TF. Parallel data sets in Table S2 suggest that bovine TF carries both Neu5Ac and Neu5Gc and mouse TF is Neu5Gc-rich, which is well in accordance with previous observations and many practices.[39,40] In addition, we further identified the linkage patterns of these sialylation modifications employing linkage-specific sialic acid esterification as previously reported.[41] Results in Figure S14 suggest that the major sialylation linkage for these TFs is α2,6 and the linkage isomer distribution is similar to each other for both Neu5Ac and Neu5Gc. Therefore, we choose to focus on the major chemical differences between Neu5Ac and Neu5Gc rather than linkage isomer in this study, although the linkage isomer could play an important regulatory role in functional sialylations.[42]

Furthermore, data sets from nontargeted AIF−MS experiments clearly track the gradual release of Neu5Ac from human TF (Figure 2A), where four Neu5Ac residues in total are captured as demonstrated by the sialylation forms F1 to F5 (Figure 2D). In contrast, AIF images of bovine TF (Figure 2B) reveal its altered sialylation form to be three Neu5Ac residues and two Neu5Gc residues (mass shift of 307 Da) (Figure 2D). Interestingly, we find that Neu5Ac is less resistant to collisional activation than Neu5Gc, which is supported by the observation of sequential and preferential release of Neu5Ac one by one that is followed by the release of Neu5Gc (Figure 2B,E). Surprisingly, it requires much higher energy to release sole Neu5Gc from mouse TF than sole Neu5Ac from human TF, as shown in Figure 2A,C, where, at 120 V, the second Neu5Ac is about to be detached while none of Neu5Gc is released. We further plotted the species changing trendlines for these sialylation isoforms against AIF voltage, as shown in Figure 2E. These semiquantitative plots add further evidence for differential sialylation releasing behavior as indicated by both the interplay between adjacent sialylation isoforms and AIF50 values to release the first sialylation (e.g., AIF50 of ∼130 V for Neu5Ac but larger than 145 V for Neu5Gc). It can thus be concluded that the Neu5Ac sialylation modification is less chemically stable than that of Neu5Gc in the case of the TF system. This observation lays important chemical foundation for the conformational stability analysis of labile sialylation modification on TFs as described below.

Conformational Stability Analysis of Differentially Sialylated Transferrin. A collision-induced unfolding (CIU)-based IM−MS analytical strategy[29,38,43,44] is employed to conduct conformational analysis among differentially sialylated TFs. TF glycoproteins with various sialylation patterns are subjected to CIU operations. Their typical unfolding fingerprints are displayed in Figures 3 and S15, and the corresponding nontargeted AIF mass spectra for apo-TFs are shown in Figures S16−S18. As shown, while multiple transitions are present in all sialylated glycoproteins, it is

https://doi.org/10.1021/acs.analchem.1c04503
Anal. Chem. 2022, 94, 2142−2153

largely seen that those TF glycoproteins experience distinct unfolding trajectories under the same activation energy range. Three TF species can be well resolved as a result of 3D classification (Figure 3M−P) in CIUSuite analysis based on their distinct unfolding trajectories (human TF, Figures 3A−D; bovine TF, Figures 3E−H; mouse TF, Figure 3I−L).

The CIU-based stepwise unfolding trajectory can both deliver conformational stability information and enable quantitative comparisons among multiple conditions through CIU50 (Supporting Information for more details) and root-mean-squared deviation (RMSD) calculation from CIU difference plots (Figure S19), respectively. The chemical structures shown in Figure 4A display the high similarity between Neu5Ac and Neu5Gc. We first calculated the CIU50 (Figure 4B) and RMSD values (Figure 4C) for three TF glycoproteins based on their individual stepwise unfolding trajectories (Figure 3).

For all charge states of TF shown in Figure 4B, we find that, human TF containing abundant Neu5Ac bears fewer transitions than bovine and mouse TF that contain fewer Neu5Ac. Although human TF surprisingly bears only two transitions in all charge states, we recommend only to compare the first three transitions during stability shift analysis, as the fourth transition is observed only in mouse TF19+ and 19+ is not the predominant conformation species (Figure S18). Fewer unfolding transitions would be indicative of lower conformational flexibility and thus relatively higher stability of the 3D arrangements in enduring external perturbations. These observations in Figure 4 indicate that human TF is most stable in resisting unfolding and has the lowest conformational flexibility.

Notably, quantitative CIU50 value-based stability analysis would be more robust compared to transition numbers. However, the CIU50 values are charge state-dependent, which means different conclusions may be drawn from different charge states when referring to conformational stability between bovine TF and mouse TF. While no statistical differences were observed from charge 18+, it can be seen that mTF shows higher conformational stability than bTF from data sets of charge 16+ (mTF with less transitions) and 17+ (mTF with higher CIU50 values). On the contrary, mTF 19+ shows lower conformational stability than bTF 19+ as indicated by the appearance of a fourth transition as well as the lower CIU50 of the transition 3 for mTF. However, the direct hTF-bTF comparison suggests that Neu5Gc modification tends to be less conformationally stable than Neu5Ac modification. This is because the sialic acids in bTF can be viewed as the replacement of one Neu5Ac from hTF with two Neu5Gc groups, but this replacement does not stabilize but instead destabilizes the protein structure compared to hTF.

As a part of conformational stability analysis, the corresponding UFS (univariate feature selection), ROC (receiver operating characteristic), and cross-validation plots for different charge states from 19+ to 16+ are shown in Figure S20, indicative of charge-dependent classification performance. Supported by this classification performance, the final 3D classification results for unfolding behavior are displayed in Figure 3M−P. The 3D plots of linear discriminants (LDs) are constructed using automatically selected CIU data having the highest classification scores. In all cases, TFs are well-separated into clusters in two-dimensional space, defined by LD1 and LD2 axis. Overall, stepwise unfolding of various TF glycoproteins shows great promise to enable unambiguously differentiation of subtle structural variations associated with sialylation effects, suggesting the gas-phase nontargeted all-ion unfolding technique as a fast and effective tool to decipher the differential roles of sialylation in regulating protein conformational stabilities.

To further assess the sialylation effects, we employ sialidase treatment to remove all sialylations and compare the conformational stability before and after sialylation removal in solution. The corresponding unfolding fingerprints and difference plots in Figures S21 and S22 clearly support that both Neu5Ac and Neu5Gc stabilize the transferrin protein structure as the unfolding occurs at higher collision voltages (higher CIU50) with sialic acid attached. Furthermore, the additional effects other than sialylation (e.g., sequence variation and *N*-glycosylation location difference) on CIU behavior can also be inferred from these sialidase treatment experiments and comparative RMSD analysis. Data in Figure S21 indicate that fully desialylated human TF has greater conformational similarity to desialylated mouse TF than that of desialylated bovine TF. Interestingly, these similarities show the same trend with sequence alignment results (Figure S1). Notably, the RMSDs for sialylated TFs (Figures 4C and S19) are much higher than those of fully desialylated TFs (Figure S21), which suggests major contribution and the importance of sialylation in affecting the unfolding fingerprints and associated stability analysis of glycoprotein TF.

Therefore, we conclude that the conformational stability of Neu5Gc modification is lower than Neu5Ac modification on glycoprotein TF; both modifications contribute to the conformational stabilization of the glycoprotein transferrin. It should be noted that the *N*-glycosylation patterns on these three TF samples we tested here differ by species, especially for human TF with two *N*-glycans while for bovine TF and mouse TF with only a single *N*-glycan attached. This type of structural difference may exert some effects on CIU behavior in addition to the abovementioned sialylation effects, although the sialidase treatment experiments have confirmed the major contributions from sialylation patterns and numbers compared to other factors including sequence variations.

Topological Stability Analysis of Differentially Sialylated Transferrin. Adding to the chemical and conformational stability interrogation on monomeric apo-TF, we also sought to understand molecular mechanisms of sialylation effects on the topological stability of holo-TF glycoproteins. We take the survey on the sialylation effects during TF dimerization because the dimerization is believed to be linked with AD development, probably through mediating the iron homeostasis of brain and co-importing of Aβ (details in Figure S1). Additionally, the dimerization of TF is relatively less investigated in previous iron metabolism studies, and the proven importance of similar transporting protein dimerization[24,45] further inspires us to initiate this set of experiments.

To do this, we performed a series of untargeted AIF experiments on holo-TF glycoproteins. As mentioned earlier, representative spectra for holo-human TF are shown in Figure S4, showing the gradual change of dimer ratios along with the elevation of AIF voltage/trap CE. Figure 4D showcases the quantitative characterization of the dimer ratio of holo-TF as a function of sialylation releasing energy, trap CE. To avoid any artifacts (e.g., nonspecific adducts and interactions) formed during nanoESI, only the dimers under activation conditions (trap CE no less than 80 V) are accounted for during the quantitative analysis. Results from Figure 4D show that both

https://doi.org/10.1021/acs.analchem.1c04503
Anal. Chem. 2022, 94, 2142−2153

human and bovine TFs tend to have a higher dimerization ratio upon the gradual releasing of sialic acids, while no significant change of the mouse TF dimer ratio is observed throughout the trap CE range. As shown in Figure 4D, the final dimerization ratio of human and bovine TFs can even grow to be 57.56 ± 4.33% (n = 3) and 44.68 ± 1.10% (n = 3), respectively, while the overall dimerization ratio of mouse TF remains 15.68 ± 2.26% (n = 3). Further examination on dimer and monomer TICs (Figure S23) confirms that the dimerization ratios increase as a function of sialylation release. A cartoon illustration of the crystal structure for human TF dimer is shown in Figure 4E to visualize the results schematically.

As a comparative study, in-solution molecular identifications of sialylation-preserved and sialylation-removed TF were carried out with both SDS PAGE and blue native PAGE.[23] Representative in-solution SDS PAGE and blue native PAGE results are shown in Figure 4F. First, SDS PAGE bands of all TF species indicated a slight decrease in molecular weight upon de-sialylation with sialidase, which is well in accordance with the native MS result (Figure 1D). Second, although several protein isoforms existed in the native PAGE results and bovine TF and mouse TF did not show noticeable changes of dimer, it is indicated that human TF bears a much higher dimer ratio after de-sialylation. The general dimerization dependency on sialylation observed from native IM−MS (Figure 4D) is in line with in-solution native PAGE results (Figure 4F), especially for the increased human TF dimer throughout the sialylation releasing processes. Taking the IM−MS data and native PAGE data together, while both Neu5Ac and Neu5Gc sialylations inhibit TF glycoprotein dimerization, the inhibiting effect of Neu5Gc cannot be recovered by sialylation release, but that of Neu5Ac was successfully recovered upon sialic acid detachment. Therefore, these observations collectively suggest that sialylation, especially Neu5Ac, effectively blocks the dimerization of TF.

CONCLUSIONS

Collectively, as shown in Table 1, our data indicate that TF sialylation enhances iron-associated Aβ cytotoxicity, promotes iron binding, stabilizes monomeric TF's gas phase conformation, and inhibits TF dimerization tendency. Considering the importance of sialylation in maintaining iron homeostasis, Neu5Ac seems to be more beneficial than Neu5Gc in terms of rescuing Aβ cytotoxicity. Given the lower chemical stability of Neu5Ac, it is unlikely that the higher conformational stability of Neu5Ac would be affected by gas-phase artifacts. The conformational stabilization of TF induced by Neu5Ac modification may be meaningful for understanding the molecular mechanisms underlying the functions of monomeric TF and even its dimerization processes that might involve the conformational rearrangements of TF.

Table 1. Brief Summary of Sialylation Effects in Aβ Cytotoxicity and TF Structural Features

sialylation dependency	SA vs DeSA[a]	Neu5Gc vs Neu5Ac
Aβ/iron/TF cytotoxicity	SA > DeSA	Neu5Gc > Neu5Ac
TF chemical stability	N. A.[b]	Neu5Gc > Neu5Ac
TF conformational stability	SA > DeSA	Neu5Gc < Neu5Ac
TF dimer stability	SA < DeSA	N. A.

[a]SA, with sialylation; DeSA, without sialylation (de-sialylated). [b]N. A., not applicable.

The observed stability differences of Neu5Ac versus Neu5Gc may be related to effective charge diversity and protein conformational variation as a function of modification site numbers, which was also reported recently on sialylation modifications.[13] While (α2,3)/(α2,6)-sialic acid linkage isomers can be differentiated by using CID with delicate data selection,[46] we do not focus on the linkage isomer effects as we believe that the difference between linkage isomers is much lower than that between Neu5Gc and Neu5Ac, which is caused by the higher degree of changes in the inherent chemical environment for hydroxy attachment.

Tentatively, we speculate that the stabilization effects by acidic sialylations (both Neu5Ac and Neu5Gc) on protein conformational stability should be related to the surface-type salt bridges between sialic acids and surrounding basic residues or other dipole elements. For example, in human TF, Asn630 sialylation may support potential salt bridge interaction with its adjacent helix dipoles in the region Lys618 to Gly628, while Asn432 sialylation may facilitate its salt bridging with Lys433. However, it is difficult to predict the salt bridge difference between Neu5Ac and Neu5Gc, as they carry the same charge numbers per modification, although the difference in total sialylation modification numbers among human, bovine, and mouse TFs would potentially affect the overall salt bridge interactions.

It should be noted that although the mechanism for brain iron importing has not been confirmed,[10,35] our results may provide some initial evidence to suggest that maintaining the monomer form (rather than dimeric form) of TF through Neu5Ac level control is crucial for its function, such as in iron homeostasis (e.g., two iron-loaded TF monomer binding to its dimeric receptor[34]) and the downstream iron-related cytotoxicity. This is because the Neu5Ac group seems to be most beneficial for rescuing Aβ cytotoxicity and simultaneously has most profound effects in inhibiting dimerization of TF, although further biological experiments need to be performed to validate this speculation and elucidate the underlying biological pathway in cells.

Our integration of a nontargeted all-ion IM−MS platform, bottom-up proteomics, in-solution evidence from native PAGE images, and MTT-based cell viability experiments have synergistically enabled the elucidation of differential roles of terminal sialylation, Neu5Ac and Neu5Gc, in regulating 3D arrangements and dimerization of glycoproteins TF from multiple species. Results herein not only provide new molecular signatures for the putative functions of terminal sialylation, but also indicate that inhibitors maintaining the Neu5Ac level at suitable values could be pursued as potential therapeutic strategies to slow the progression of several sialylated glycoprotein-linked diseases, including AD.[5]

ASSOCIATED CONTENT

Supporting Information

The Supporting Information is available free of charge at https://pubs.acs.org/doi/10.1021/acs.analchem.1c04503.

Additional experimental details including the calculation of lab-frame CE, proposed Aβ escape routes from endosome following cellular uptake via TF, rationale behind the IM−MS study, glycoform list as identified

https://doi.org/10.1021/acs.analchem.1c04503
Anal. Chem. 2022, 94, 2142−2153

from three TFs, and other supporting evidence for sialylation effects on the TF protein structure (PDF)

AUTHOR INFORMATION

Corresponding Authors

Gongyu Li − *Research Center for Analytical Science and Tianjin Key Laboratory of Biosensing and Molecular Recognition, College of Chemistry, Nankai University, Tianjin 300071, China;* orcid.org/0000-0002-2367-4433; Email: ligongyu@nankai.edu.cn

Lingjun Li − *School of Pharmacy and Department of Chemistry, University of Wisconsin-Madison, Madison, Wisconsin 53706, United States;* orcid.org/0000-0003-0056-3869; Email: Lingjun.li@wisc.edu

Authors

Ashley Phetsanthad − *Department of Chemistry, University of Wisconsin-Madison, Madison, Wisconsin 53706, United States*

Min Ma − *School of Pharmacy, University of Wisconsin-Madison, Madison, Wisconsin 53706, United States*

Qinying Yu − *School of Pharmacy, University of Wisconsin-Madison, Madison, Wisconsin 53706, United States*

Ashita Nair − *School of Pharmacy, University of Wisconsin-Madison, Madison, Wisconsin 53706, United States*

Zhen Zheng − *School of Pharmacy, Tianjin Medical University, Tianjin 300070, China*

Fengfei Ma − *School of Pharmacy, University of Wisconsin-Madison, Madison, Wisconsin 53706, United States; Protein Sciences, Discovery Biologics, Merck & Co., Inc., South San Francisco, California 94080, United States*

Kellen DeLaney − *Department of Chemistry, University of Wisconsin-Madison, Madison, Wisconsin 53706, United States*

Seungpyo Hong − *School of Pharmacy, University of Wisconsin-Madison, Madison, Wisconsin 53706, United States;* orcid.org/0000-0001-9870-031X

Complete contact information is available at: https://pubs.acs.org/10.1021/acs.analchem.1c04503

Author Contributions

G.L. and L.L. designed research, G.L. and A.P. performed MS-related research, M.M. performed cell experiments, Q.Y. performed bottom-up proteomics experiments, A.N. did PAGE experiments, and G.L. and L.L. wrote the paper. All authors contributed to discussion of the data and have reviewed and approved the final manuscript.

Notes

The authors declare no competing financial interest.

ACKNOWLEDGMENTS

The authors would like to thank Professor Dick Zare from Stanford University and Professor Brandon Ruotolo from the University of Michigan for providing insightful discussions and suggestions. The authors gratefully appreciate Dr. Yu Gao and Dr. Xinyu Zhao (Waisman Center, UW-Madison) for their generous providing of cell lines. This work was funded in part by NIH (R01DK071801, R56DK071801, U01CA231081, R21AG065728, and RF1AG052324), and NSF (CHE-1710140 and CHE-2108223). The Orbitrap instruments were purchased through the support of an NIH shared instrument grant (NIH-NCRR S10RR029531) and the University of Wisconsin−Madison, Office of the Vice Chancellor for Research and Graduate Education with funding from the Wisconsin Alumni Research Foundation. K.D. acknowledges the National Institutes of Health-General Medical Sciences F31 National Research Service Award (1F31GM126870-01A1) for funding. L.L. acknowledges a Vilas Distinguished Achievement Professorship and Charles Melbourne Johnson Distinguished Chair Professorship with funding provided by the Wisconsin Alumni Research Foundation and University of Wisconsin−Madison School of Pharmacy. G.L. thanks the Nankai University start-up funding support through the Fundamental Research Funds for the Central Universities (no. 020/63213057).

REFERENCES

(1) Kaneko, Y.; Nimmerjahn, F.; Ravetch, J. V. *Science* **2006**, *313*, 670−673.

(2) Sumer-Bayraktar, Z.; Kolarich, D.; Campbell, M. P.; Ali, S.; Packer, N. H.; Thaysen-Andersen, M. *Mol. Cell. Proteomics* **2011**, *10*, M111 009100.

(3) Otto, V. I.; Schürpf, T.; Folkers, G.; Cummings, R. D. *J. Biol. Chem.* **2004**, *279*, 35201−35209.

(4) Marotta, N. P.; Lin, Y. H.; Lewis, Y. E.; Ambroso, M. R.; Zaro, B. W.; Roth, M. T.; Arnold, D. B.; Langen, R.; Pratt, M. R. *Nat. Chem.* **2015**, *7*, 913−920.

(5) Schedin-Weiss, S.; Winblad, B.; Tjernberg, L. O. *FEBS J.* **2014**, *281*, 46−62.

(6) van Rensburg, S. J.; Berman, P. A.; Potocnik, F. C. V.; Taljaard, J. J. F. *Metab. Brain Dis.* **2000**, *15*, 243−247.

(7) Taniguchi, M.; Okayama, Y.; Hashimoto, Y.; Kitaura, M.; Jimbo, D.; Wakutani, Y.; Wada-Isoe, K.; Nakashima, K.; Akatsu, H.; Furukawa, K.; Arai, H.; Urakami, K. *Dementia Geriatr. Cognit. Disord.* **2008**, *26*, 117−122.

(8) Connor, J. R.; Menzies, S. L.; St. Martin, S. M.; Mufson, E. J. *J. Neurosci. Res.* **1992**, *31*, 75−83.

(9) Lu, C.-D.; Ma, J.-K.; Luo, Z.-Y.; Tai, Q.-X.; Wang, P.; Guan, P.-P. *Aging* **2018**, *10*, 3117−3135.

(10) Luck, A. N.; Mason, A. B. *Curr. Top. Membr.* **2012**, *69*, 3−35.

(11) Chen, Z.; Yu, Q.; Yu, Q.; Johnson, J.; Shipman, R.; Zhong, X.; Huang, J.; Asthana, S.; Carlsson, C.; Okonkwo, O.; Li, L. *Mol. Cell. Proteomics* **2021**, *20*, 100081.

(12) Wu, D.; Struwe, W. B.; Harvey, D. J.; Ferguson, M. A. J.; Robinson, C. V. *Proc. Natl. Acad. Sci. U.S.A.* **2018**, *115*, 8763−8768.

(13) Yen, H. Y.; Liko, I.; Gault, J.; Wu, D.; Struwe, W. B.; Robinson, C. V. *Angew. Chem., Int. Ed.* **2020**, *59*, 15560−15564.

(14) Ghanbari, Z.; Housaindokht, M. R.; Bozorgmehr, M. R.; Izadyar, M. *J. Theor. Biol.* **2016**, *404*, 73−81.

(15) Guillot, A.; Dauchez, M.; Belloy, N.; Jonquet, J.; Duca, L.; Romier, B.; Maurice, P.; Debelle, L.; Martiny, L.; Durlach, V.; Baud, S.; Blaise, S. *Sci. Rep.* **2016**, *6*, 35666.

(16) Kawabata, H. *Free Radical Biol. Med.* **2019**, *133*, 46−54.

(17) Arosio, P.; Ingrassia, R.; Cavadini, P. *Biochim. Biophys. Acta* **2009**, *1790*, 589−599.

(18) Soding, J. *Bioinformatics* **2005**, *21*, 951−960.

(19) Bernhard, O. K.; Kapp, E. A.; Simpson, R. J. *J. Proteome Res.* **2007**, *6*, 987−995.

(20) Spik, G.; Debruyne, V.; Montreuil, J.; van Halbeek, H.; Vliegenthart, J. F. G. *FEBS Lett.* **1985**, *183*, 65−69.

(21) Caslavska, J.; Lanz, C.; Burda, P.; Tobler, M.; Thormann, W. *J. Sep. Sci.* **2017**, *40*, 2488−2497.

(22) Conrad, M.; Pratt, D. A. *Nat. Chem. Biol.* **2019**, *15*, 1137−1147.

(23) Wittig, I.; Braun, H.-P.; Schägger, H. *Nat. Protoc.* **2006**, *1*, 418−428.

(24) Choi, T. S.; Lee, H. J.; Han, J. Y.; Lim, M. H.; Kim, H. I. *J. Am. Chem. Soc.* **2017**, *139*, 15437−15445.

(25) Ruotolo, B. T.; Benesch, J. L. P.; Sandercock, A. M.; Hyung, S.-J.; Robinson, C. V. *Nat. Protoc.* **2008**, *3*, 1139−1152.

(26) Bush, M. F.; Hall, Z.; Giles, K.; Hoyes, J.; Robinson, C. V.; Ruotolo, B. T. *Anal. Chem.* **2010**, *82*, 9557−9565.
(27) Marklund, E. G.; Degiacomi, M. T.; Robinson, C. V.; Baldwin, A. J.; Benesch, J. L. P. *Structure* **2015**, *23*, 791−799.
(28) Li, G.; DeLaney, K.; Li, L. *Nat. Commun.* **2019**, *10*, 5038.
(29) Eschweiler, J. D.; Rabuck-Gibbons, J. N.; Tian, Y.; Ruotolo, B. T. *Anal. Chem.* **2015**, *87*, 11516−11522.
(30) Marty, M. T.; Baldwin, A. J.; Marklund, E. G.; Hochberg, G. K. A.; Benesch, J. L. P.; Robinson, C. V. *Anal. Chem.* **2015**, *87*, 4370−4376.
(31) Varkouhi, A. K.; Scholte, M.; Storm, G.; Haisma, H. J. *J. Controlled Release* **2011**, *151*, 220−228.
(32) Raditsis, A. V.; Milojevic, J.; Melacini, G. *Biophys. J.* **2013**, *105*, 473−480.
(33) Liu, B.; Moloney, A.; Meehan, S.; Morris, K.; Thomas, S. E.; Serpell, L. C.; Hider, R.; Marciniak, S. J.; Lomas, D. A.; Crowther, D. C. *J. Biol. Chem.* **2011**, *286*, 4248−4256.
(34) Belaidi, A. A.; Bush, A. I. *J. Neurochem.* **2016**, *139*, 179−197.
(35) Hare, D.; Ayton, S.; Bush, A.; Lei, P. *Front. Aging Neurosci.* **2013**, *5*, 34.
(36) Bousejra-ElGarah, F.; Bijani, C.; Coppel, Y.; Faller, P.; Hureau, C. *Inorg. Chem.* **2011**, *50*, 9024−9030.
(37) Valensin, D.; Migliorini, C.; Valensin, G.; Gaggelli, E.; La Penna, G.; Kozlowski, H.; Gabbiani, C.; Messori, L. *Inorg. Chem.* **2011**, *50*, 6865−6867.
(38) Zhong, Y.; Han, L.; Ruotolo, B. T. *Angew. Chem., Int. Ed.* **2014**, *53*, 9209−9212.
(39) Pinho, S. S.; Reis, C. A. *Nat. Rev. Cancer* **2015**, *15*, 540−555.
(40) Moremen, K. W.; Tiemeyer, M.; Nairn, A. V. *Nat. Rev. Mol. Cell Biol.* **2012**, *13*, 448−462.
(41) Reiding, K. R.; Blank, D.; Kuijper, D. M.; Deelder, A. M.; Wuhrer, M. *Anal. Chem.* **2014**, *86*, 5784−5793.
(42) Zhuo, Y.; Bellis, S. L. *J. Biol. Chem.* **2011**, *286*, 5935−5941.
(43) Shelimov, K. B.; Jarrold, M. F. *J. Am. Chem. Soc.* **1997**, *119*, 2987−2994.
(44) Tian, Y.; Han, L.; Buckner, A. C.; Ruotolo, B. T. *Anal. Chem.* **2015**, *87*, 11509−11515.
(45) Fang, T.; Chen, W.; Sheng, Y.; Yuan, S.; Tang, Q.; Li, G.; Huang, G.; Su, J.; Zhang, X.; Zang, J.; Liu, Y. *Nat. Commun.* **2019**, *10*, 186.
(46) Pett, C.; Nasir, W.; Sihlbom, C.; Olsson, B.-M.; Caixeta, V.; Schorlemer, M.; Zahedi, R. P.; Larson, G.; Nilsson, J.; Westerlind, U. *Angew. Chem., Int. Ed.* **2018**, *57*, 9320−9324.

https://doi.org/10.1021/acs.analchem.1c04503
Anal. Chem. 2022, 94, 2142−2153